W(CO)6 in cryogenic solids: A comparative study of vibrational properties

Raphaël Thon, Wutharath Chin, Didier Chamma, Alejandro Gutiérrez Quintanilla, Michele Chevalier, Jean-Pierre Galaup, Claudine Crépin

$W(CO)_6$ in cryogenic solids: A comparative study of vibrational properties

Raphaël Thon[a,1], Wutharath Chin[a,*], Didier Chamma[a], Alejandro Gutiérrez-Quintanilla[a], Michèle Chevalier[a], Jean-Pierre Galaup[b], Claudine Crépin[a]

[a] *Institut des Sciences Moléculaires d'Orsay, CNRS, Univ. Paris-Sud, Université Paris-Saclay, F-91405 Orsay (France)*
[b] *Laboratoire Aimé Cotton, CNRS, ENS Cachan, Univ. Paris-Sud, Université Paris-Saclay, F-91405 Orsay (France)*

Abstract

A comparative study of the vibrational properties of $W(CO)_6$ has been performed in different solids at cryogenic temperatures focusing on the IR absorption and the vibrational dynamics of the CO stretching mode of the organometallic compound. Guest-host interactions are investigated in doped solids through the linear IR spectroscopy and four-wave mixing techniques at different temperatures. We show how the host nature, the trapping site, the crystallographic ordering affect the properties of the guest molecule and in particular its vibrational dynamics.

Keywords: photon echo; vibrational dynamics; cryogenic solids

1. Introduction

The advent of picosecond (ps) and femtosecond (fs) laser sources in the IR domain has enabled the study of the vibrational dynamics of a wide variety of systems spanning from biological molecules [1, 2, 3, 4, 5] to material sciences [6, 7, 8] through nonlinear four-wave mixing techniques such as IR photon echo [9] or two-dimensional IR spectroscopy [10]. Thanks to the very large transition dipole

*Corresponding author
Email address: wutharath.chin@u-psud.fr (Wutharath Chin)
[1] Present address: CNRS Formation Entreprises, Bât. 31, Avenue de la Terrasse, 91198 Gif-sur-Yvette Cedex (France)

moment (μ = 1 D) of the asymetric CO stretch vibrational mode (T_{1u} mode near 2000 cm^{-1}) $W(CO)_6$ organometallic complex is highly interesting since it yields a large nonlinear response. In this sense $W(CO)_6$ has been widely studied by means of nonlinear processes in various condensed media [11, 12, 13]. In particular $W(CO)_6$ represents a very sensisitive probe to characterize guest-host interactions and allows a very detailed insight into environment effects induced by the nature of the host on the molecular dynamics of $W(CO)_6$. We have investigated the environment effects on the vibrational properties of $W(CO)_6$ in the condensed phase in different cryogenic lattices such as rare gas crystals (argon [13], krypton [14]) and molecular hosts (nitrogen [14], methane [15]).

The vibrational properties of $W(CO)_6$ have been measured by linear and nonlinear (pump-probe and photon echo techniques) IR spectroscopy at different temperatures. We thus have access to T_1 population relaxation time and T_2 dephasing time. T_2 is related to the homogeneous broadening γ_{homo} through the relation:

$$\gamma_{homo} = \frac{1}{\pi T_2} = \frac{1}{2\pi T_1} + \frac{1}{\pi T_2 *} \tag{1}$$

where $T_2{}^*$, called pure dephasing time, is especially sensitive to the environment. In order to get an overview of the vibrational behavior of $W(CO)_6$ in cryogenic lattices, we performed additional experiments in neon (for probing a third rare gas host), in parahydrogen (a specific host with quantum properties) and in carbon tetrafluoride (following the series of methane solids CH_4 and CD_4). This paper is thus dedicated to the comparison of these various results allowing for conclusive remarks on the host dependence of $W(CO)_6$ vibrational properties. After a brief description of the experimental procedures, the results in the different hosts are summarized. They are discussed in the last part before the conclusions in terms of host effects on the absorption features, vibrational population relaxation and dephasing processes. We show how the host nature, the trapping site, the crystallographic ordering affect the properties of the guest molecule and in particular its vibrational dynamics. The conclusions highlight

the main tendencies obtained from the comparison of all the results.

2. Experimental procedure and methods

The detailed experimental set-ups have been extensively described in our previous papers [14, 16] and only the main descriptions related to new results are presented.

In the case of CF_4, as for the experiments described in Refs. [14, 15] the matrix samples have been obtained by continuous deposition of a gaseous mixture onto a cold CaF_2 window of the cryostat. Gaseous samples are prepared at room temperature by mixing $W(CO)_6$ (Sigma Aldrich) with the carrier gas with $[W(CO)_6]/[Host]$ ratio varying from 10^{-5} to 10^{-3}. Matrix thickness is kept below 100 μm. Concentration and deposition times are adapted to keep an optical density of the T_{1u} mode of $W(CO)_6$ of ≈ 1. Deposition temperatures can vary between 15 and 30 K depending on the host (30 K for CF_4).

Nonlinear measurements are obtained using an IR OPA source for fs pulses (see ref. [14] for details). The fs IR OPA is combined to a 3-pulse photon echo set-up. It is pumped by a 800 nm Ti:Sa laser/amplifier system and delivers an IR pulse centered at 1980 cm^{-1}, bandwidth 150 cm^{-1}, duration 145 fs, output ≈ 3 μJ. Resulting IR beam is then split into three beams ($\boldsymbol{k_1}$, $\boldsymbol{k_2}$ and $\boldsymbol{k_3}$ wave vectors) of equivalent intensities using two coated ZnSe beamsplitters. The echo signal is emitted in a well-defined direction given by phase-matching such as $\boldsymbol{k}_s=\boldsymbol{k_3}+\boldsymbol{k_2}-\boldsymbol{k_1}$. The signal beam is focused on an MCT (mercury cadmium telluride) detector. There are two independant delay stages giving access to two delay times τ and T, called coherence time and waiting time and corresponding to the delay between the first two pulses and the last two pulses, respectively. The detected signal (quadratic detection) is:

$$S(\tau,T)=\int_0^\infty dt\left|P^{(3)}(\tau,T,t)\right|^2 \qquad (2)$$

$P^{(3)}(\tau,T,t)$ is the third order polarization created in the sample with the wave vector $\boldsymbol{k}_s$. In a rough way, the *S(T)* signal at fixed τ gives access to T_1 population

lifetime and $S(\tau)$ signal at fixed T to dephasing processes through the measure of T_2 dephasing time.

Absorption spectra have been recorded using an FTIR Mattson spectrometer at $0.25\,\mathrm{cm}^{-1}$ spectral resolution to check the quality of the sample and its evolution with temperature and time. A switching gold coated mirror brings the FTIR globar beam to probe the same matrix region as in photon echo experiments. Linear and nonlinear data have been measured using the same nitrogen-cooled MCT detector.

Additional experiments in neon and parahydrogen (pH_2) have been performed with another set-up dedicated to pH_2 experiments. Hydrogen is converted to parahydrogen in a first cryostat kept at 17 K and parahydrogen vapor is directly condensed onto a cold diamond window of a second cryostat (IceOxford) at the lowest temperature of 3 K. $W(CO)_6/pH_2$ samples are obtained by flowing pH_2 over a tube containing $W(CO)_6$ and carrying its vapor before the deposition. The experimental procedure to produce doped pH_2 samples is the same as that described in ref. [17]. $W(CO)_6$/Ne samples are obtained in the same manner, replacing hydrogen by neon and keeping the first cryostat at 40 K to avoid any neon condensation. In this case, the first cryostat is used to trap all residual impurities. IR spectra of the samples are recorded by means of a Nicolet FTIR spectrometer at $0.125\,\mathrm{cm}^{-1}$ spectral resolution. No time-resolved measurements have been conducted with this cryogenic set-up.

3. Results

3.1. Rare gas matrices: Ar, Kr, Ne

$W(CO)_6$ has been isolated in Ar, Kr and Ne solids. The IR spectra have been recorded in the three hosts and photon echo experiments have been performed in Ar and Kr. The IR spectrum in Kr and Ne in the region of the asymetric νCO stretch of $W(CO)_6$ is displayed in Figure 1. Spectra reveal a complex absorption spreading over $10\,\mathrm{cm}^{-1}$ in contrast to the gas phase where there is only one line at $1998\,\mathrm{cm}^{-1}$ [18]. The complex structure reflects the complexity of

the trapping sites. With a diameter around 0.78 nm, $W(CO)_6$ is a huge impurity to trap in these cristallographic lattices. Rare gas solids have an *fcc* structure with a nearest neighbors distance d of 0.40, 0.38 and 0.32 nm for Kr, Ar and Ne respectively, i.e. much smaller than the size of $W(CO)_6$. Consequently, the guest molecule is trapped in multi-vacancy sites. The structure of the absorption spectra can result from two effects: the presence of many different trapping sites (differing for example by the number of hosts removed), and the possible degeneracy removal of the T_{1u} mode (triply degenerated in the isolated molecule) in trapping sites of lower degree of symmetry than O_h group (the group of symmetry of the isolated molecule).

Because Kr, Ar and Ne have different lattice parameters, trapping sites should be different in the three hosts. In that sense, the Ar spectrum seems the simplest and could reflect a smaller number of different trapping sites, i.e. a better match between the size of $W(CO)_6$ and that of the vacancies [13]. Nevertheless spectra in the three rare gas solids show a major structure in the red side and a minor one in the blue side. The energy gap between these two bands is roughly $5\pm2\,\mathrm{cm}^{-1}$ with no obvious correlation with the lattice parameter. In Ne, the absorption spectrum spreads only over $8\,\mathrm{cm}^{-1}$ and this gap is reduced to $\approx 3\,\mathrm{cm}^{-1}$ (Figure 1). The frequency shift between matrix and gas phase ($1998\,\mathrm{cm}^{-1}$) is also the smallest. This is a well-known consequence of the lowest polarizability of Ne which induces the smallest matrix effect on the transition frequencies of guest molecules.

No significant change is observed when varying the temperature in Ar [13] and Kr [14] in terms of band position or linewidth. On the contrary, annealing at 60 K in Kr leads to reorganization of the trapping sites yielding a small change in the relative intensities of the bands. We have also observed slight differences in $W(CO)_6$/Ar spectra when varying the experimental deposition conditions. However the relative intensities of the two main features remain constant. The IR spectroscopy in Ne has been recorded at 3, 6 and 8 K and no change has been observed.

Despite complex band structures, the vibrational dynamics in Kr and Ar

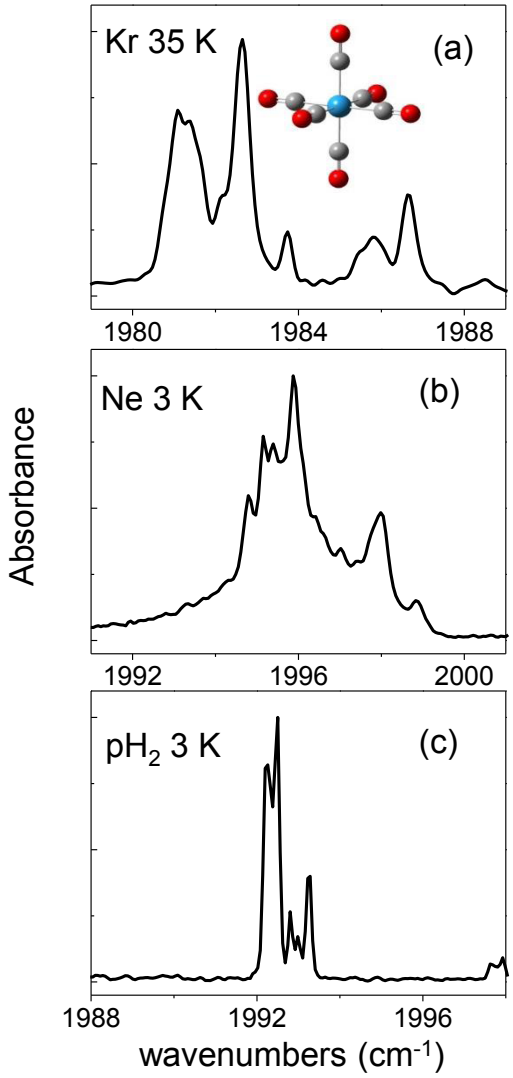

Figure 1: IR spectra of $W(CO)_6$ in (a) Kr (35 K), (b) Ne (3 K) and (c) pH_2 (3 K). The inset shows a schematic of $W(CO)_6$ (W in blue, C in grey, O in red).

occur to be rather simple. Time-resolved signals measuring T_1 and T_2 always exhibit long decay times in the hundreds of ps. Of course, since the IR laser pulses are spectrally broad, the time-resolved signals correspond to the nonlinear response of the entire absorption spectra. In Kr, there is no variation in the population decays when changing the temperature. The decay is not in fact mono-exponential and the *S(T)* signals are better fitted with two exponential contributions that take into account two different dynamics linked to the population relaxation from $v = 1$ excited state (T_1) and recovery to the ground state (T_g), suggesting a long-lived intermediate level in the vibrational relaxation. We find $T_1 = 80 \pm 20$ ps and $T_g \approx 1.5$ ns [14]. In Ar, a single exponential is found but the signal has not been recorded until the end of the relaxation, suggesting that the long T_g time has not been actually measured. It gives a T_1 population relaxation time which slightly shortens when temperature increases with $T_1 >$ 200 ps at 8 K and $T_1 = 160$ ps at 20 K [13].

Similarly to *S(T)*, the *S(τ)* signals in Kr show no temperature effects between 25 and 50 K. The decay of the signal yields 100 ± 20 ps, equivalent to a γ_{homo} homogeneous broadening of $0.106\,\mathrm{cm}^{-1}$. It is smaller than the width of the narrowest lines of the absorption spectrum (FWHM$\approx 0.5\,\mathrm{cm}^{-1}$): it means that the absorption structure is not composed of homogeneous substructures. In Ar, T_2 values are slightly longer than in Kr, they are not constant with temperature but they are in the same order of magnitude with T_2 (8 K) = 400 ps and T_2 (20 K) = 200 ps. Corresponding γ_{homo} of 0.026 and 0.053 cm^{-1} are much less than the linewidths of the absorption structures ($\approx 2.3\,\mathrm{cm}^{-1}$). In both rare gas solids we find T_2 comparable to twice T_1, meaning that dephasing processes are essentially governed by population relaxation.

3.2. Molecular matrices

3.2.1. Nitrogen and methane

We have studied nitrogen and methane solids because the crystals also adopt an *fcc* structure similar to rare gas solids. Moreover, nearest neighbors distances d are of the same order of magnitude, and in particular close to that of Kr lattice:

$d = 0.401$ nm and 0.417 nm in N_2 and CH_4 respectively. It is thus expected that the geometry of the trapping sites are similar between these molecular solids and Kr solids. In the case of CH_4, our experimental conditions allow the exploration of different phases. CH_4 solid presents two crystalline phases (both of *fcc* structure) with a temperature of phase transition at 20.4 K at zero pressure. From 20.4 K to 90.7 K phase I is orientationally disordered and molecules occupy O_h symmetry sites. Below 20.4 K in phase II, there is partial ordering of CH_4 molecules due to octupole-octupole interactions with 3/4 of molecules undergoing hindered rotation in D_{2d} symmetry and 1/4 free rotation in O_h symmetry [19].

The IR absorption of $W(CO)_6$ in N_2 and CH_4 is quite complex and displays structured bands as in the case of Ne, Ar and Kr. As previously, spectra show two main features centered at 1984 and 1989 cm^{-1} in N_2 and 1981 and 1987 cm^{-1} in CH_4 (frequency gap $\approx 5\,cm^{-1}$, as in Kr). Main differences from rare gas matrices stem from the strong temperature dependence of the IR spectra (Figure 2). Temperature effects have been of great help to assign the different substructures. In both molecular solids, four bands or substructures can be distinguished (numbered 1 to 4 in Figure 2). In N_2 only band 2 exhibits a strong and reversible temperature effect while intensities of the three other bands remain almost constant. These characteristics suggest that bands 1, 3 and 4 correspond to the three components of the vibrational T_{1u} mode in sites of low symmetry. Band 2 would then correspond to sites of high symmetry where the molecule keeps its O_h symmetry [14]. In spite of a more complex absorption structure in CH_4, the comparison with N_2 also leads to assign bands 1, 3 and 4 to low symmetry sites and band 2 to high symmetry sites [15]. Populations of high and low-symmetry sites are comparable in N_2 and CH_4 with a ratio of 40:60 and 45:55 respectively. The temperature broadening of band 2 in N_2 could be due to an expected homogeneous broadening and time-resolved measurements confirm this assumption (see below). Very surprisingly, the temperature behavior seems reversed in CH_4 as highlighted in Figure 2. In fact, bands 1, 2 and 3 are found to coalesce from phase II to phase I, leading to a global narrowing when

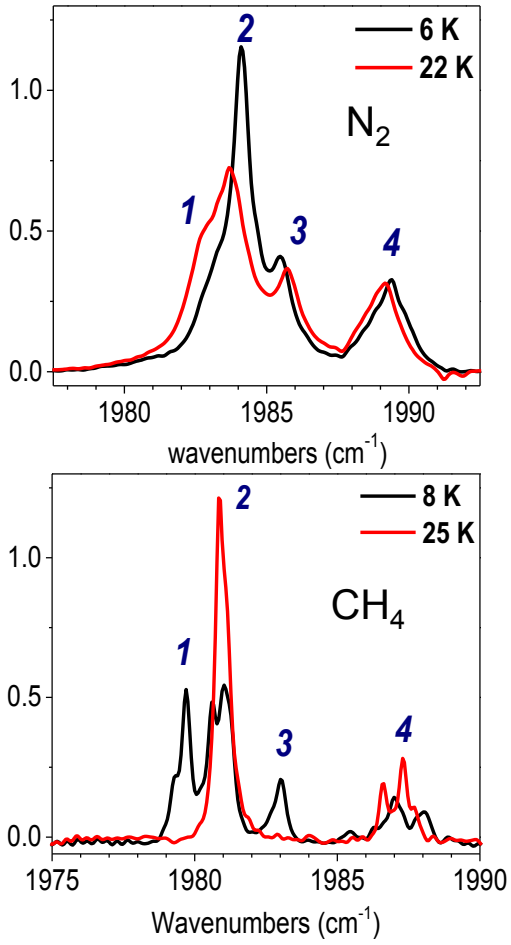

Figure 2: IR spectra of $W(CO)_6$ in N_2 at 6 and 22 K and CH_4 at 8 and 22 K. Low and high temperatures are respectively plotted as black and red traces.

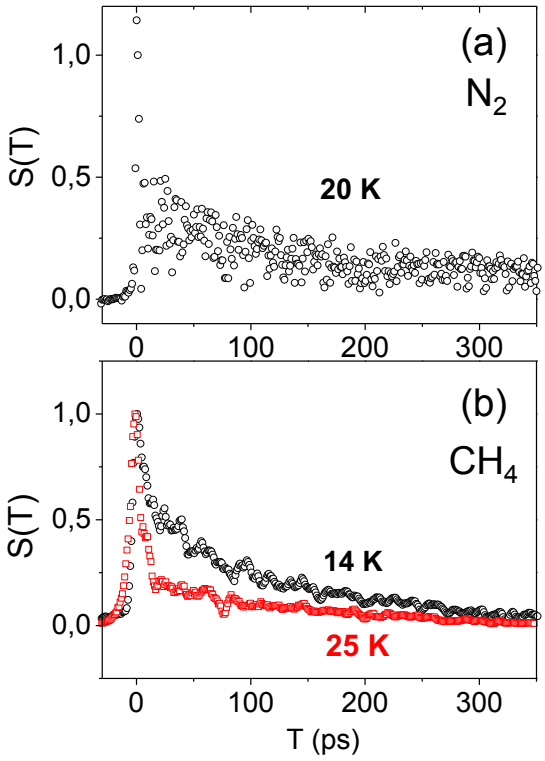

Figure 3: *S(T)* signals (normalized) of $W(CO)_6$ in (a) N_2 at 20 K and (b) CH_4 at 14 K (black) and 25 K (red). The very steep rise ("spike") at T = 0 is due to additional nonlinear signals produced when the IR pulses simultaneously arrive onto the sample. It is not related to the probed dynamics [21].

temperature increases [15]. This effect is assigned to a motional narrowing due to the complete rotational disorder and the large motional fluctuations of CH_4 hosts in phase I, which for this reason is also named plastic phase [20].

There is no obvious temperature effect on the vibrational population relaxation of $W(CO)_6$ in N_2 and the decay times are in the hundreds of ps, similarly to the case of Kr (Figure 3a). As in Kr two times in the population decay can also be considered, a T_1 time around 180 ps and a very long recovery time T_g > 1 ns [14]. They represent averaged population decay times for all the sites as in Kr and Ar. On the contrary, a strong temperature effect is observed in

CH_4 in the *S(T)* signals corresponding to distinct dynamical behaviours above and below phase transition of CH_4 (Figure 3b): there is one long component around 200 ps at all temperatures (same order of magnitude as T_1 in N_2) but there is an additional shorter decay of 10 ps in phase I (red trace in Figure 3b). The weight of the short component corresponds to the weight of high symmetry sites obtained in the analysis of the absorption spectra. Our analysis of the time-resolved signals suggests that the short 10 ps component reflects T_1 time of $W(CO)_6$ molecules in these high symmetry sites [15]. In these sites, $W(CO)_6$ does not significantly perturb the CH_4 lattice and fast relaxation involving a methane vibron can occur in phase I because of the strong broadening of methane modes in this crystallographic phase. Note that, whatever the temperature no very long (> 400 ps) decay has been measured in CH_4 precluding the existence of a very long T_g time.

Photon echo measurements in N_2 and CH_4 both exhibit temperature effects. Figure 4 shows signals recorded at 9 and 20 K in N_2 and at 8 and 24 K in CH_4. Experimental curves in N_2 are correctly modelled when considering T_2 times that depend on the family of sites. Only T_2 times of high symmetry sites are strongly temperature dependent: they vary from 130 ps at 6 K to 15 ps at 20 K. It is in perfect agreement with the temperature broadening of band 2 in the absorption, leading to a significant homogeneous contribution at 20 K. In low symmetry sites, T_2 is almost constant, around 50 ps, i.e. shorter than in rare gas matrices. The temperature dependence in high symmetry sites can be described as an enhancement of the homogeneous width by coupling with a libration mode of the nitrogen lattice [14].

In CH_4, beside the large shortening of the population relaxation time in phase I assigned to high symmetry sites, T_2 is found to decrease with temperature increase in all sites. It is well depicted in Figure 4b where *S(τ)* signals have been measured with long waiting times (T > 30 ps) to get rid of this short 10 ps component in T_1 in phase I. T_2 times are found to decrease smoothly from 120-140 ps at 6 K to 25-30 ps at 30 K. The latter value is very close to twice T_1 of high symmetry sites, where dephasing is governed by the loss of population

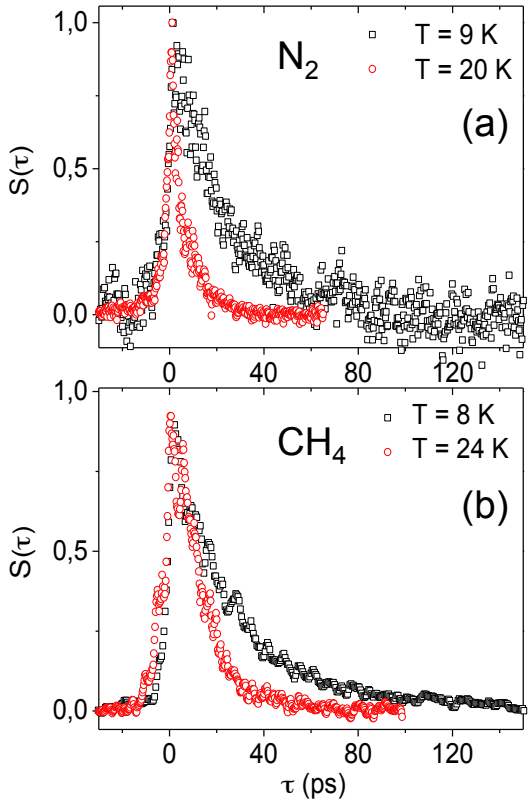

Figure 4: *S(τ)* signals (normalized) of $W(CO)_6$ in (a) N_2 and (b) CH_4. Red circles and black squares represent signals at high (20 and 24 K) and low (8 and 9 K) temperatures respectively.

in phase I. The corresponding homogeneous width of $\approx 0.4\,\mathrm{cm}^{-1}$ at 30 K for all sites is consistent with a predominant homogeneous broadening with a bandwidth of $0.5\,\mathrm{cm}^{-1}$ measured on the main component of the absorption spectrum at 30 K. In both N_2 and CH_4 solids, the *S(τ)* signal becomes more symmetric with respect to τ (Figure 4) reflecting the increase of the homogeneous contribution to broadening but one can notice that, whereas the rise of the signal (at $\tau < 0$) does not depend on temperature in N_2, it is longer at high temperature in CH_4 indicating that the inhomogeneous contribution is simultaneously reduced, which is a signature of the motional narrowing [15].

Experiments have also been conducted in heavy methane (CD_4) for which two phase transitions can be explored. In fact, the T_{1u} mode of $W(CO)_6$ is found in resonance with the $2\nu_4$ overtone mode of CD_4 [15]. The consequence is a very fast population relaxation at all temperatures (≈10 ps) which prevents any analysis of environment effects on pure dephasing processes in this solid. The absorption spectrum shows the same global structure as in CH_4, with broad features in all the phases, suggesting a similar analysis based on low and high symmetry sites with a high/low ratio in CD_4 of 55:45.

3.2.2. Carbon tetrafluoride CF_4

In order to probe another crystallographic environment with molecular "spherical" hosts, we have studied CF_4 solid after CH_4 and CD_4. CF_4 carbon tetrafluoride presents a phase transition at 76.2 K (at zero pressure) [22], the high- and low-temperature phases are respectively designated by I and II. Phase I (or β) is also named "plastic" phase due to orientational disorder of CF_4 molecules [23], similarly to CH_4. It corresponds to a rhomboedric structure. Phase II (or α) is a well-ordered crystal and the lattice structure changes to monoclinic [24]. It is therefore an interesting medium for trapping $W(CO)_6$ in terms of lattice structure and orientation of molecules.

In fact, only phase II has been explored in our experiments. Attempts to measure spectra above 50 K failed due to low optical density of the sample because of evaporation of the CF_4 matrix at 55 K despite a melting point at

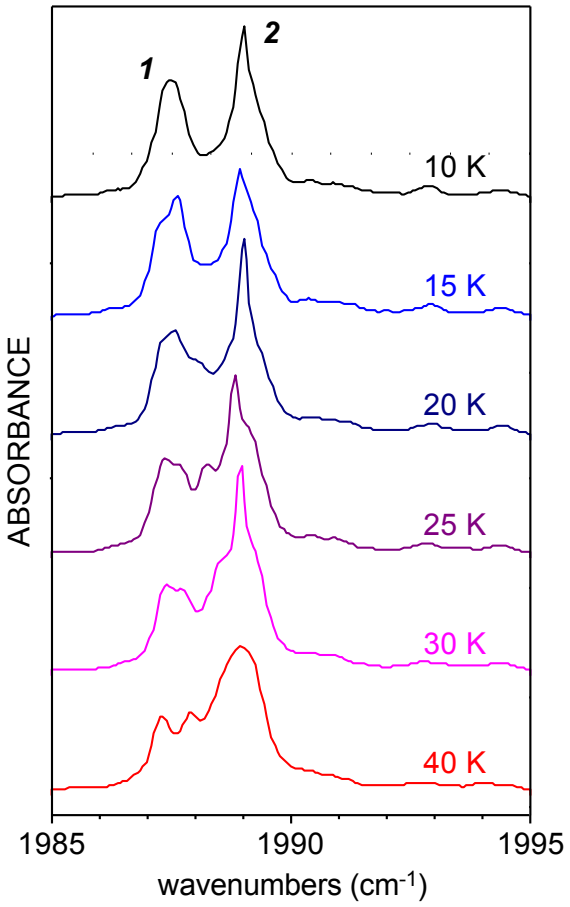

Figure 5: IR spectra of $W(CO)_6$ in CF_4 from 10 K to 40 K (top to bottom).

89.5 K. This can be due to local heating of the matrix by the light sources. The IR spectrum is temperature dependent, as shown in Figure 5 between 10 and 40 K. At low temperature (8 K) it exhibits two main bands centered at 1987.5 and 1989 cm^{-1} (bands 1 and 2) and weaker bands at 1992.9 and 1994.4 cm^{-1}. The temperature dependence of the two main bands is especially pronounced. Band 1 at 1987.5 cm^{-1} broadens and shows a more and more obvious structure from 8 to 20 K. It seems to contain a substructure that shifts to the blue, reaching the middle of the two bands around 22 K and joining band 2 at higher temperatures. The consequence is a red shift and an increase of band 2 at 1989 cm^{-1} with temperature. At 35 K, there is only one main band at 1988.7 cm^{-1}. It is found to narrow slightly from 8 to 20 K and to broaden because of the previous effect. Spectral changes observed when varying the temperature are reversible. CF_4 forms a larger "sphere" (0.43 nm diameter) than methane but as in the other solids studied, $W(CO)_6$ (0.78 nm diameter) replaces more than one host in the lattice. Because of the monoclinic structure in phase II, the O_h symmetry of $W(CO)_6$ cannot be preserved and band splitting due to degeneracy removal is expected. It is thus not surprising that the spectral behavior is different in CF_4. Anyway, the comparison with the observations in N_2 and CH_4 suggests that the most intense band 2 at 1989 cm^{-1} contains the main components of highest symmetry sites. The frequency shift of some components in the absorption spectrum toward the main one when temperature increases looks like the band coalescence observed in CH_4 from phase II to phase I [15], although 35 K is rather far from the temperature of phase transition in CF_4. One must remind that a lowering of this temperature was observed in methane when the solid was doped with $W(CO)_6$ [15] and such effect can also occur in CF_4.

Unfortunately, time-resolved measurements have been very difficult to obtain due to high scattering of the samples. The best signals have been recorded in a short temperature range only (30-45 K) corresponding to the best quality samples so only global behaviors can be extracted from the signals. Nevertheless a clear shortening of T_2 upon temperature increase is observed. T_2 of 50 ps $\pm$ 10 ps is obtained between 10 and 20 K, and this value continuously decreases to

≈ 20 ps at 50 K. The *S(τ)* signal at 30 K is shown in Figure 6 a. The asymmetric profile indicates a predominant inhomogeneous contribution to broadening. The deduced value of $T_2 = 38$ ps is an average for all bands. It corresponds to a homogeneous broadening of $0.27\,\mathrm{cm}^{-1}$, which is lower than the linewidth of the substructures ($0.5 - 1\,\mathrm{cm}^{-1}$) measured in the absorption spectra. The *S(τ)* profile seems obviously more symmetric at 50 K (not shown), corresponding to the IR spectrum involving only one main band. T_1 is measured in the hundreds of ps in the explored temperature range, without any clear temperature effect. An example is given in Figure 6b at 35 K, yielding $T_1 = 240$ ps $\pm$ 30 ps. No obvious long component can be extracted from the *S(T)* curves, suggesting that there is no long T_g recovery time as in CH_4. Similarly to the case of N_2, no population relaxation enhancement takes place in CF_4 while a pure dephasing time T_2* in the tens of ps as given by eq. 1 is present, that is temperature dependent. The molecular nature of the host could be at play in pure dephasing process, as in N_2 and CH_4 but data are too scattered for a more precise conclusion.

3.3. Quantum matrix: parahydrogen pH₂

Only IR measurements are available in solid parahydrogen (pH_2). Parahydrogen is a very attractive environment as it possesses unique properties. It is a quantum crystal thanks to its light pH_2 mass and to the significant translational zero-point motion of the pH_2 molecules about their equilibrium positions within the solid. The weak pH_2-pH_2 intermolecular forces, the $J = 0$ rotational state at cryogenic temperatures for all molecules, the spherical symmetry of the ground state, the minimal cage effect contribute to the "softness" of the matrix and result in weak perturbations on the guest molecules [25]. By trapping $W(CO)_6$ molecules in pH_2 we thus expect that its spectroscopy and dynamics will qualitatively differ from the other solids studied so far. Solid pH_2 adopts an *hcp* lattice structure with nearest neighbors distance $d = 0.379$ nm, i.e. a value very close to that of solid Ar. $W(CO)_6$ should thus replace a similar number of pH_2 hosts as Ar atoms in the respective lattices. Because of its softness, site effects are usually strongly reduced in this quantum solid and absorption bands

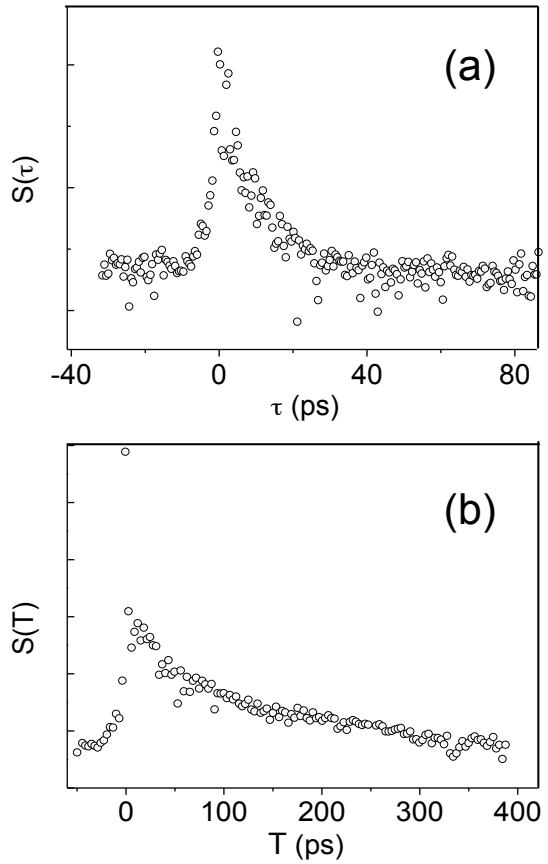

Figure 6: Examples of time-resolved signals in CF_4 doped with $W(CO)_6$ (arbitrary units), (a) *S(τ)* at 30 K, $T = 20$ ps, (b) *S(T)* at 35 K ("spike" at the origin as in Figure 3a).

are expected to be homogeneously broadened [26, 27, 28].

The IR spectrum of $W(CO)_6$ isolated in pH_2 at 3 K is displayed in Figure 1c. It is simpler than in the other solids and the global feature is much narrower than in other hosts. However, it does not show a unique band, as in the isolated molecule but two doublets. The most intense doublet absorbs at 1992.2 and 1992.5 cm^{-1} and the weakest one is located at 1992.8 and 1993.3 cm^{-1}. The absorption spectrum exhibits a very slow time evolution, with a decrease of the bands at 1993.3 and 1992.5 cm^{-1} meaning that they correspond to metastable sites. The two weaker bands have half intensities of the two stronger ones. We conclude that the two doublets correspond to two sites where the triply degenerated T_{1u} mode gives rise to two components, one being doubly degenerated (the strongest one). Such degeneracy removal is consistent with the *hcp* structure. Bands are very narrow and their actual linewidth cannot be reached with our FTIR resolution (FWHM $< 0.125\,cm^{-1}$). It gives a $0.1\,cm^{-1}$ limit to the value of γ_{homo}. The corresponding T_2 dephasing time is thus longer than 100 ps. Time-resolved experiments are necessary to obtain more accurate values.

4. Discussion

4.1. Spectroscopy

The complex structures in the absorption spectra in the crystalline cryogenic solids mainly reflect site effects. In amorphous solids, like xerogels or glasses, only a non structured and broad absorption band has been observed [16, 30, 31]. Since this band is inhomogeneously broadened, it corresponds to a continuum of different sites. Results in differents environments are summarized in Table 1. The analysis of the structures in N_2 and CH_4 suggests the existence of high symmetry sites where the O_h symmetry of $W(CO)_6$ is preserved [14, 15]. In *fcc* lattices, with nearest neighbors distances around 0.4 nm, O_h (or T_d) trapping sites large enough to contain the guest molecule are obtained when removing 13 hosts (one and its 12 nearest neighbors). The size of this big hole has a diameter of around 0.77 nm, which is well adapted to $W(CO)_6$. Therefore,

Table 1: Summary of the results on the vibrational properties for the main features of $W(CO)_6$ in different environments.

Host	T (K)	Absorption (cm^{-1})		T_1 (ps)	T_2 (ps)	References
		Major feature	Minor feature			
Ar	7-8	1986	1991	240-270	400 ± 80	Ref. [13]
	20	1986	1991	160 ± 10	200 ± 40	
Kr	25	1983.9	1989.3	80 ± 20 & > 1000 (T_g)	100 ± 20	Ref. [14]
Ne	$3 \rightarrow 8$	1995.9	1999	not measured		
N_2	6	1984.1	1989.3	180 ± 30 & > 1000 (T_g)	130 (high sym.) & 50 (low sym.)	Ref. [14]
	20	1983.7	1989	180 ± 30 & > 1000 (T_g)	15 (high sym.) & 50 (low sym.)	
CH_4	6	1980.6	1987.0	200 (low sym.)	130	Ref. [15]
	25	1980.8	1986.6	10 (high sym.) & 200 (low sym.)	30	
CD_4	$15 \rightarrow 30$	1980.5	1986.3	≤ 10	10	Ref. [15]
CF_4	$20 \rightarrow 50$	1989	1992.9	240	38	this work
pH_2	3	1992.5	1993.3	not measured		
CCl_4	300	1978		800	< 1	Ref. [29]
dibutyl-phtalate	$0 \rightarrow 300$	1982		33	$33 \rightarrow 13$	Ref. [11]
xerogels	4.5	1982		60-70	28	Ref. [16]
	300				4	

these "O_h" trapping sites should also exist in Ar and Kr matrices and possibly in Ne. Similarly to the case of N_2 and CH_4, we can also conclude that in all these *fcc* solids the weaker feature in the blue part of the spectra is assigned to a non degenerated component of the T_{1u} mode of $W(CO)_6$ in low symmetry sites. A rough estimation of the integrated absorption of the weak and the strong bands (separated by few wavenumbers) can give an idea of the ratio of high/low symmetry sites. We find 40:60, 45:55, 45:55 in Kr, Ar and Ne respectively, it is as expected very similar to the 40:60 and 45:55 ratios obtained in the spectral analysis in N_2 and CH_4 respectively. The *hcp* structure of pH_2 is very close to the previously described *fcc* structure and with a nearest neighbors distance d of 0.379 nm, a hole of 13 pH_2 could also fit for the trapping of $W(CO)_6$. The symmetry of such trapping site is D_{3h} in the *hcp* structure, explaining the splitting of the T_{1u} mode in two components. The results in pH_2 in that sense confirm the previous assignment.

Figure 7a shows the IR spectra of $W(CO)_6$ in the different solids studied, CH_4, Kr, N_2, Ar, CF_4, pH_2 and Ne from top to bottom. All these features are red-shifted from the gas phase frequency ($1998\,cm^{-1}$) [18], meaning that the gas to matrix shift is due to dispersive interactions. In Figure 7b is plotted the T_{1u} frequency measured in the different media as a function of the polarizability α of the host. It clearly shows a correlation between T_{1u} position and α, except for CF_4. The weakest feature observed in all hosts is less down shifted from the gas phase. It corresponds to a CO stretch mode in a specific direction in low symmetry sites that is either weakly perturbed by the environment, or more sensitive to constraints as in Ne, where it is slightly above the gas phase value because of a more compact lattice ($d = 0.32$ nm) inducing more repulsive forces than in the other hosts. The red-shift of the T_{1u} frequency in the condensed phase can reach 20 cm^{-1} [30], i.e. 1% of its value. The anharmonicity of this mode has been measured in various environments by means of oscillations observed in photon echo signals and has been assigned to quantum beats between the $v = 0 \leftrightarrow v = 1$ and $v = 1 \leftrightarrow v = 2$ transitions [11]. The anharmonicity value measured in N_2 is 14.7 cm^{-1} [14], 14.5 cm^{-1} in CH_4 [15], $14.5\,cm^{-1}$ in

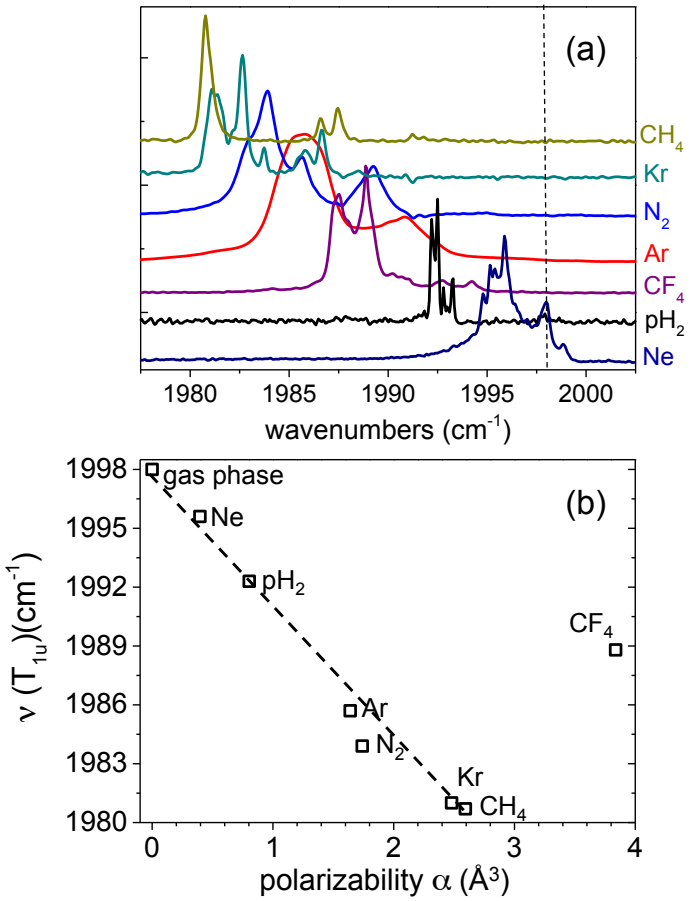

Figure 7: (a) IR spectra of $W(CO)_6$ recorded in the region of T_{1u} mode in, from top to bottom, CH_4, Kr, N_2, Ar, CF_4, pH_2 and Ne. Temperature is 20 K for all solids except in pH_2 and Ne where it is 3 K. The gas phase frequency ($1998\,cm^{-1}$) is marked with a dotted line. (b) ν wavenumber (in cm^{-1}) of the T_{1u} mode of $W(CO)_6$ in the gas phase, Ne, pH_2, Ar, Kr, N_2, CH_4 and CF_4 plotted as a function of the polarizability α of the host (Å^3).

xerogels [16], 14.7 cm^{-1} in dibutylphtalate [11]. These values differ by 1.5%, to be compared with the 0.2% dispersion found for the corresponding fundamental frequencies.

4.2. Population relaxation

Vibrational relaxation of $W(CO)_6$ in liquids was found to be strongly solvent dependent [32] because the vibrational pattern of the solvent can give intermediate levels in the vibrational relaxation depending on the vibrational energies of its modes compared to the probed T_{1u} mode of $W(CO)_6$. The same is observed in cryogenic solids. In CD_4 a vibrational mode of the host is in quasi-resonance with the T_{1u} mode yielding a reduced T_1 value of 10 ps. We also suggest that the vibron of CH_4 at 1538 cm^{-1} can be efficiently involved in the population relaxation of $W(CO)_6$ in high symmetry sites because this energy corresponds to the energy gap between the probed T_{1u} mode and low energy modes of $W(CO)_6$ around 400 cm^{-1}, leading also to a strongly reduced T_1 time [15]. In all the other cases studied, T_1 of 100-200 ps has been measured. In particular, T_1 is not shortened in phase II of CH_4 nor in low symmetry sites despite a rich vibrational pattern below 1900 cm^{-1}. At low temperature, the population relaxation pathway needs to include vibrational levels of the host of rather precise energies to be efficient. The same remark is verified in the case of CF_4. The solid possesses indeed only vibrational fundamental modes of low energies ($\leq$ 1320 cm^{-1}) [23] which cannot fill the gap between the T_{1u} mode and low energy modes of $W(CO)_6$ [33].

The temperature dependence of the long T_1 (100-200 ps) has been difficult to measure, with very weak changes in the short temperature range accessible in the experiments. Because of the experimental difficulties to obtain precise measurements (low laser and sample stabilities in long acquisitions of hundreds of ps), signal changes are usually in the measurement errors. A slight effect has been measured in Ar without the possibility to extract a temperature law. It means that lattice phonons are rather inefficient in the relaxation pathway, which is expected since the order of magnitude of their energy is once or twice

lower than the probed vibration.

On the other hand, 100-200 ps values are short compared with T_1 = 800 ps obtained in CCl_4 at room temperature [29]. There is no obvious reason for T_1 times to be shorter in matrices at temperatures below 20 K, especially in rare gas solids or N_2 with no vibrational levels below 1900 cm^{-1}. In these solids, a longer time (> 1 ns) has been measured and assigned to T_g recovery time. This value compares well with the long T_1 recorded in CCl_4. Assuming that this T_g time would correspond to the lifetime of $v = 1$ in these cryogenic solids, the shorter T_1 would then be assigned to the population relaxation time of the component of the T_{1u} mode probed in the four wave mixing experiment, i.e. the time to leave the level probed by the first pulse and probably to reach another component of the T_{1u} mode (through intra molecular energy transfer). Components of the T_{1u} mode differ by less than few wavenumbers, which is lower than energies of phonons. It explains that this vibrational energy transfer is itself inefficient. Considering that T_g times are T_{1u} lifetimes in rare gas and N_2 solids, our experiments therefore show that the lifetime in CH_4 and in CF_4 is reduced (no long T_g has been detected) as expected because of the existence of vibrational mode of medium energies. The T_1 value (< 100 ps) found in xerogels at low temperature is consistent with this latter assumption [16].

4.3. Dephasing processes

Photon echo experiments give a direct access to the vibrational dephasing times. Thanks to the measurements of the population relaxation times, pure dephasing times are extracted by means of eq. 1. From the results reported in cryogenic solids, there are two kinds of environments where dephasing processes are governed by population relaxation. The first one is rare gas solids (Ar and Kr). Both T_1 and T_2 times are in the hundreds of ps in the explored temperature range. Because of quite large measurement errors, it is not possible to extract valuable values of T_2* times, but in any case, at any temperature, we can conclude that T_2* is longer than twice T_1. Population relaxation is fast in the second kind of environment as in CD_4, where $T_1 \leq 10$ ps and $T_2 \approx 10$ ps,

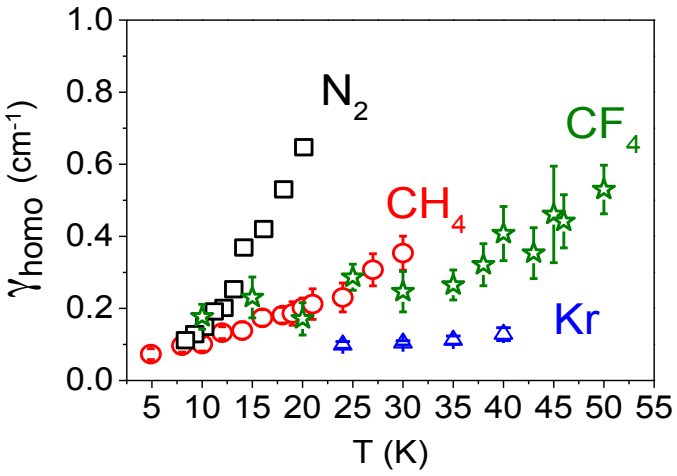

Figure 8: Plot of γ_{homo} as a function of temperature in Kr rare gas solid (triangles) and in N_2 (squares), CH_4 (circles), CF_4 (stars) molecular hosts.

giving T_2* longer than 20 ps, i.e. longer than twice T_1. In the high symmetry sites of CH_4 in phase I, T_2 cannot be measured separately from the response of low symmetry sites but our signals are in full agreement with estimations of T_2 and T_2* equal to the above values in CD_4. Otherwise, T_2 and T_2* in CH_4 out of these specific environments are always longer than 20 ps. In the other cryogenic environments, T_2 is found shorter than T_1 and efficient pure dephasing processes occur ($T_2^* < T_1$) due to the environment. The first important remark is that it happens only with molecular hosts.

The temperature dependence of T_2 and T_2* documents the processes at play in the vibrational dephasing. This temperature dependence is clearly observed in N_2 and CH_4. In N_2, it concerns the temperature evolution of dephasing time in high symmetry sites. It has not been possible to extract a clear temperature dependence of T_2 or T_2* in the other sites whereas T_1 and T_2 values clearly indicate that pure dephasing processes occur also in these sites. In contrast in CH_4, the temperature behavior can be followed in low symmetry sites because fast population relaxation at high temperatures in high symmetry sites hides pure dephasing processes. As in N_2 and CH_4, pure dephasing processes are also

at play in CF_4 solid. Figure 8 displays the evolution of γ_{homo}, linked to T_2, against temperature in high symmetry sites of N_2 and low symmetry sites of CH_4 compared with CF_4 and Kr rare gas solid. In the latter increase of γ_{homo} with temperature is very weak, being more or less included in the error bars. It means that phonons related to the hosts translational motion are hardly coupled with the vibrational motion of the guest. In contrast, the strong temperature dependence in high symmetry sites of N_2 where the dephasing processes at play are due to coupling with a librational mode of the solid. The behavior observed in CH_4 and CF_4 lies between the two cases, showing the clear influence of the molecular motions in the dephasing processes.

5. Conclusions

By probing the vibrational properties of a guest molecule ($W(CO)_6$) in diverse cryogenic lattices, we have obtained several results highlighting the specificities of the different environments explored. The IR absorption of $W(CO)_6$ always exhibits a structured feature. It is a signature of the limited number of families of trapping sites due to the crystalline environment. The simplest structure is observed in solid pH_2, a solid with specific properties minimizing site effects. Band broadening of each structure in pH_2 is expected to be homogeneous but no time-resolved experiment has yet been measured to confirm this assumption. In other cryogenic matrices, some substructures possess narrow linewidths ($\approx 0.5\,\mathrm{cm}^{-1}$) but time-resolved experiments always show a significant inhomogeneous contribution to broadening. However strong homogeneous broadening is clearly observed in the absorption when temperature increases in a fraction of N_2 trapping sites.

Relaxation processes are found to be host-dependent and they are moreover site dependent as proved in N_2 or CH_4. Except in the case of resonances between the probed vibration and the energy levels in the host + guest system, T_1 population relaxation times are long. In fact, values of 100-200 ps may reflect vibrational energy transfers between components of the T_{1u} mode of $W(CO)_6$

when a very long time in the ns range is detected, that would correspond to the $v = 1$ lifetime (as observed in rare gas and N_2 solids). Dephasing is enhanced in molecular hosts probably because of coupling between molecular motions. Acoustic phonons turn out to be very inefficient in the dephasing process, in contrast with phonons coming from rotational or vibrational motions of the molecular hosts. Librons and vibrons affect the vibrational dynamics and their effect appears to be strong in sites where the lattice is weakly perturbed, i.e. high symmetry sites.

Acknowledgements

This research was supported by the RTRA Triangle de la Physique grants no. 2010-004-T NOSTADYNE, 2012-053T DYMA and 2013-0436T REACMAQ. The authors are grateful to Justinas Ceponkus for his help in the parahydrogen measurements. They also thank Bernard Bourguignon and Aimeric Ouvrard for the use of femstosecond laser system and their technical support.

References

[1] R. M. Hochstrasser, Special feature on Multidimensional ultrafast spectroscopy, Proceedings of the National Academy of Sciences 104 (36) (2007) 14190.

[2] H. S. Chung, Z. Ganim, K. C. Jones, A. Tokmakoff, Transient 2D IR spectroscopy of ubiquitin unfolding dynamics., Proceedings of the National Academy of Sciences of the United States of America 104 (36) (2007) 14237–42.

[3] E. H. G. Backus, R. Bloem, P. M. Donaldson, J. A. Jhalainen, R. Pfister, B. Paoli, A. Caflisch, P. Hamm, 2D-IR study of a photoswitchable isotope-labeled alpha-helix, Journal of Physical Chemistry B 114 (10) (2010) 3735–3740.

[4] A. Ghosh, J.-J. Ho, A. L. Serrano, D. R. Skoff, T. Zhang, M. T. Zanni, Two-dimensional sum-frequency generation (2D SFG) spectroscopy: summary of principles and its application to amyloid fiber monolayers, Faraday discussions 177 (2015) 493–505.

[5] M. R. Panman, C. N. van Dijk, H. Meuzelaar, S. Woutersen, Communication: Nanosecond folding dynamics of an alpha helix: Time-dependent 2D-IR cross peaks observed using polarization-sensitive dispersed pump-probe spectroscopy, The Journal of Chemical Physics 142 (4) (2015) 041103.

[6] P. M. Donaldson, P. Hamm, Gold nanoparticle capping layers: Structure, dynamics, and surface enhancement measured using 2D-IR spectroscopy, Angewandte Chemie - International Edition 52 (2) (2013) 634–638.

[7] R. D. Mehlenbacher, M.-Y. Wu, M. Grechko, J. E. Laaser, M. S. Arnold, M. T. Zanni, Photoexcitation dynamics of coupled semiconducting carbon nanotube thin films., Nano Letters 13 (4) (2013) 1495–501.

[8] M. Grechko, Y. Ye, R. D. Mehlenbacher, T. J. McDonough, M.-Y. Wu, R. M. Jacobberger, M. S. Arnold, M. T. Zanni, Diffusion-Assisted Photoexcitation Transfer in Coupled Semiconducting Carbon Nanotube Thin Films, Nature Communications 8 (6) (2014) 5383–5394.

[9] W. H. Hesselink, D. A. Wiersma, Picosecond Photon Echoes Stimulated from an Accumulated Grating, Physical Review Letters 43 (27) (1979) 1991–1994.

[10] M. C. Asplund, M. T. Zanni, R. M. Hochstrasser, Two-dimensional infrared spectroscopy of peptides by phase-controlled femtosecond vibrational photon echoes., Proceedings of the National Academy of Sciences of the United States of America 97 (15) (2000) 8219–8224.

[11] A. Tokmakoff, D. Zimdars, R. S. Urdahl, R. S. Francis, A. S. Kwok, M. D. Fayer, Infrared vibrational photon echo experiments in liquids and glasses, The Journal of Physical Chemistry 99 (36) (1995) 13310–13320.

[12] K. D. Rector, M. D. Fayer, Vibrational echoes: A new approach to condensed-matter vibrational spectroscopy, International Reviews in Physical Chemistry 17 (3) (1998) 261–306.

[13] M. Broquier, C. Crépin, H. Dubost, J. P. Galaup, IR spectra and vibrational dephasing of the CO stretching mode in W(CO)6 doped cryogenic matrices, Chemical Physics 341 (1-3) (2007) 207–217.

[14] R. Thon, W. Chin, J.-P. Galaup, A. Ouvrard, B. Bourguignon, C. Crépin, Vibrational Perturbations of W(CO)6 Trapped in a Molecular Lattice Probed by Linear and Nonlinear Spectroscopy., The Journal of Physical Chemistry A 117 (2013) 8145–8156.

[15] R. Thon, W. Chin, D. Chamma, J. P. Galaup, A. Ouvrard, B. Bourguignon, C. Crépin, Vibrational spectroscopy and dynamics of W(CO)6 in solid methane as a probe of lattice properties, The Journal Chemical Physics submitted.

[16] J. P. Galaup, M. Broquier, C. Crépin, H. Dubost, J. M. Ortega, F. Chaput, J. P. Boilot, Vibrational dynamics of CO stretching in W(CO)6-doped hybrid xerogels from 5 K to room temperature with the CLIO-FEL, Journal of Luminescence 86 (3) (2000) 363–370.

[17] J. Ceponkus, W. Chin, M. Chevalier, M. Broquier, A. Limongi, C. Crépin, Infrared study of glycolaldehyde isolated in parahydrogen matrix., The Journal of Chemical Physics 133 (9) (2010) 094502.

[18] L. H. Jones, Vibrational spectra and force constants of the hexacarbonyls of chromium, molybdenum and tungsten, Spectrochimica Acta 19 (1) (1963) 329–338.

[19] W. Press, A. Kollmar, CH4: tunneling states, rotations, and phase transition in a quantum molecular crystal, Solid State Communications 17 (1975) 405–408.

[20] D. G. Bounds, M. L. Klein, G. N. Patey, Molecular dynamics simulation of the plastic phase of solid methane, The Journal of Chemical Physics 72 (10) (1980) 5348.

[21] P. Hamm, Coherent effects in femtosecond infrared spectroscopy, Chemical Physics 200 (3) (1995) 415–429.

[22] Y. A. Sataty, A. Ron, F. H. Herbstein, Carbon tetrafluoride - phase II: Far infrared spectrum and crystal structure, The Journal Chemical Physics 62 (3) (1975) 1094–1097.

[23] R. P. Fournier, R. Savoie, F. Bessette, A. Cabana, Vibrational Spectra of Liquid and Crystalline CF4, The Journal of Chemical Physics 49 (3) (1968) 1159–1164.

[24] A. N. Fitch, J. K. Cockcroft, The structure of solid carbon tetrafluoride, Zeitschrift fur Kristallographie 203 (1993) 29–39.

[25] I. F. Silvera, The solid molecular hydrogens in the condensed phase: Fundamentals and static properties, Reviews of Modern Physics 52 (2) (1980) 393–452.

[26] T. Momose, H. Katsuki, H. Hoshina, N. Sogoshi, High-resolution laser spectroscopy of methane clusters trapped in solid parahydrogen, The Journal of Chemical Physics 107 (19) (1997) 7717–7720.

[27] K. Yoshioka, D. T. Anderson, Infrared spectra of CH3F(ortho-H2)n clusters in solid parahydrogen, The Journal of Chemical Physics 119 (9) (2003) 4731–4742.

[28] T. Momose, H. Hoshina, M. Fushitani, H. Katsuki, High-resolution spectroscopy and the analysis of ro-vibrational transitions of molecules in solid parahydrogen, Vibrational Spectroscopy 34 (1) (2004) 95–108.

[29] A. Tokmakoff, B. Sauter, M. D. Fayer, Temperature-Dependent Vibrational-Relaxation in Polyatomic Liquids: Picosecond Infrared Pump-

Probe Experiments, The Journal of Chemical Physics 100 (12) (1994) 9035–9043.

[30] E. Heilweil, R. Cavanagh, J. Stephenson, Population relaxation of CO (v=1) vibrations in solution phase metal carbonyl complexes, Chemical Physics Letters 134 (2) (1987) 181–188.

[31] A. Tokmakoff, R. S. Urdahl, D. Zimdars, R. S. Francis, A. S. Kwok, M. D. Fayer, Vibrational spectral diffusion and population dynamics in a glass-forming liquid: Variable bandwidth picosecond infrared spectroscopy, The Journal of Chemical Physics 102 (10) (1995) 3919.

[32] A. Tokmakoff, M. D. Fayer, Homogeneous Vibrational Dynamics and Inhomogeneous Broadening in Glass-Forming Liquids - Infrared Photon-Echo Experiments from Room-Temperature to 10 K, The Journal of Chemical Physics 103 (8) (1995) 2810–2826.

[33] R. Amster, R. Hannan, M. Tobin, Vibrational spectra of some group VI hexacarbonyls, Spectrochimica Acta 19 (9) (1963) 1489–1494.

Figure captions

Figure 1 IR spectra of $W(CO)_6$ in (a) Kr (35 K), (b) Ne (3 K) and (c) pH_2 (3 K). The inset shows a schematic of $W(CO)_6$ (W in blue, C in grey, O in red).

Figure 2 IR spectra of $W(CO)_6$ in N_2 at 6 and 22 K and CH_4 at 8 and 22 K. Low and high temperatures are respectively plotted as black and red traces.

Figure 3 *S(T)* signals (normalized) of $W(CO)_6$ in (a) N_2 at 20 K and (b) CH_4 at 14 K (black) and 25 K (red). The very steep rise ("spike") at T = 0 is due to additional nonlinear signals produced when the IR pulses simultaneously arrive onto the sample. It is not related to the probed dynamics [21].

Figure 4 *S(τ)* signals (normalized) of $W(CO)_6$ in (a) N_2 and (b) CH_4. Red circles and black squares represent signals at high (20 and 24 K) and low (8 and 9 K) temperatures respectively.

Figure 5 IR spectra of $W(CO)_6$ in CF_4 from 10 K to 40 K (top to bottom).

Figure 6 Examples of time-resolved signals in CF_4 doped with $W(CO)_6$ (arbitrary units), (a) *S(τ)* at 30 K, T = 20 ps, (b) *S(T)* at 35 K ("spike" at the origin as in Figure 3a).

Figure 7 (a) IR spectra of $W(CO)_6$ recorded in the region of T_{1u} mode in, from top to bottom, CH_4, Kr, N_2, Ar, CF_4, pH_2 and Ne. Temperature is 20 K for all solids except in pH_2 and Ne where it is 3 K. The gas phase frequency (1998 cm^{-1}) is marked with a dotted line. (b) ν wavenumber (in cm^{-1}) of the T_{1u} mode of $W(CO)_6$ in the gas phase, Ne, pH_2, Ar, Kr, N_2, CH_4 and CF_4 plotted as a function of the polarizability α of the host ($Å^3$).

Figure 8 Plot of γ_{homo} as a function of temperature in Kr rare gas solid (triangles) and in N_2 (squares), CH_4 (circles), CF_4 (stars) molecular hosts.